R. & M. No. 2613
(12,130)
A.R.C. Technical Report

MINISTRY OF SUPPLY

AERONAUTICAL RESEARCH COUNCIL
REPORTS AND MEMORANDA

Boundary-Layer and Wake Investigation in Supersonic Flow

By

J. Lukasiewicz and J. K. Royle

LONDON: HER MAJESTY'S STATIONERY OFFICE
1952
SIX SHILLINGS NET

Boundary-Layer and Wake Investigation in Supersonic Flow

By

J. LUKASIEWICZ and J. K. ROYLE

COMMUNICATED BY THE PRINCIPAL DIRECTOR OF SCIENTIFIC RESEARCH (AIR)
MINISTRY OF SUPPLY

Reports and Memoranda No. 2613*

October, 1948

Summary.—The report describes the results of traverses of the boundary-layer and wake encountered in a small supersonic tunnel at a Mach number of 2·5.

The tunnel was arranged with two throats in parallel formed by two shaped walls enclosing a shaped central element.

Both the laminar and turbulent boundary-layers were encountered and compared with existing experimental and theoretical results.

The frictional drag of the central element as deduced from the wake traverses is in close agreement with that calculated from considerations of laminar boundary-layer growth over the surface of the element.

The tests also provide information relating to the design of nozzle profiles, particularly at the point of inflexion, where the changes of pressure gradient may have a serious effect on the boundary-layer and on the velocity distribution.

1. *Introduction.*—Recent tests on a two-dimensional multiple-throat nozzle consisting of eleven small nozzles placed in parallel and mounted in a 5·5 × 5·5 in. supersonic wind-tunnel[1] indicated that a more refined investigation of the growth and strength of the wakes, arising from the nozzle elements, was desirable.

It was also convenient to combine the wake traverses with a systematic set of traverses of the boundary-layer along a tunnel wall.

The tests, therefore, were arranged to supply quantitative values against which the various theories of the compressible boundary layer could be checked.

From the boundary-layer traverses, the velocity profiles of both the laminar and turbulent layers have been measured and compared with existing experimental and theoretical data of the compressible boundary-layer along a flat plate in the absence of a pressure gradient; while the wake traverses have provided a check on the calculations of the laminar boundary-layer over the nozzle profile, *i.e.*, in accelerated flow.

The visual results of flow within the nozzle elements and the theoretical calculations have also provided further information on the flow in the region of the point of inflexion of the nozzle profile.

* R.A.E. Report Aero. 2292. S.D.31. Received 3rd February, 1949.

2. *Experimental Arrangement.*—2.1. *Supersonic wind-tunnel.*—The tests were conducted in a small vertical supersonic wind-tunnel, Figs. 1, 2, 3, consisting of a double nozzle formed by a shaped cylindrical element* between two shaped walls (*see* Fig. 4), and followed by slightly diverging straight liners. The nozzle and diverging duct sections were enclosed by parallel glass walls (1·73 in. apart) through which the whole length of supersonic flow in the tunnel could be observed. At the nozzle end the glass was drilled, and the central nozzle element was held in position by two screws. In order to secure the nozzle element thin rubber washers were inserted between the glass and the nozzle element and shaped washers were fitted on the outer side of the windows. When assembling the tunnel a special gauge was used to align the nozzle assembly.

The nozzle profile is given in Fig. 4; it is a scaled-down profile of a Kochel wind tunnel nozzle for a nominal Mach number of 2·48.

Schlieren and shadow observations of flow in the wind tunnel were made and photographs were taken.

2.2. *Measurements.*—The main measurements consisted of pitot-traverses of the boundary-layer on the tunnel walls and of the wake produced by the central nozzle element. The traversing gear, incorporating a micrometer head, is shown in detail in Fig. 5 and can be seen mounted in the tunnel in Fig. 2.

The traverses were made at four positions, designated A, B, C and D, at various distances from the nozzle as indicated in Fig. 3. In addition, the stagnation pressure P_0 and temperature T_0 at the nozzle entry and static pressure (P) at nine points along the flat liners (stations a, b . . . . i, Fig. 3) were recorded.

2.3. *Static Pressure Distribution.*—The distribution of the static pressure in the tunnel, corresponding to a total divergence of the flat liners of 2 in 100 (1·15 deg), which was adopted in the tests, is shown in Fig. 8 for various air humidities. In the tests, air dried by cooling to a temperature of about — 30 deg C was used; the effect of humidity is clearly seen in Fig. 8.

In all cases, the static pressure decreases downstream of the nozzle exit, attains an approximately constant mean value downstream of station d, and again increases at point i. The observed fluctuations of the static pressure can be attributed to three causes: (i) non-uniformity of flow distribution due to the nozzle profile, (ii) disturbances originating from the trailing edge of the centre profile and joints between the nozzle and flat liners and (iii) waviness of flat liners. It appears that all these factors played a part in the case described. The flow distribution in a full-scale nozzle of the same profile was subsequently measured and it was found that, due to a discontinuous change of curvature at the inflexion point (transition from circular throat to the profile determined by characteristics), a strong expansion-shock disturbance was propagated downstream. The sudden change in the density gradient originating from the point of inflexion is clearly visible in the schlieren photograph of the flow, Fig. 7; also the computed velocity distribution along the centre profile surface, Fig. 18, shows a very abrupt decrease in the acceleration at the inflexion point.

As regards (ii), the disturbances originating from the trailing edge and from the end of the nozzle liners are seen in the schlieren photograph, Fig. 7. The latter could not be completely eliminated by careful adjustments of the setting of the flat liners relative to the nozzle exit surface.

At a Mach number of 2·5, a 0·5 deg deflection of flow produces a 3 per cent change in the static pressure, so that any waviness of the surfaces of wooden liners would result in appreciable disturbances. As mounted, the wooden liners could be distorted by uneven packing and tightening of fixing screws and care was taken to obtain as plane surfaces as possible.

* The shape of the central cylindrical element was the same as in the multiple-throat nozzle block previously tested.

During the traverses static pressure readings were taken at frequent intervals, and it was found that, due to disturbances caused by the pitot-tube holder, static pressures downstream of the traverse stations varied considerably depending on the pitot-tube position. Typical results for ' B ' traverse are shown in Fig. 9, the static pressure distribution being plotted for pitot-tube holder fully inside the tunnel (pitot-tube at the wall opposite to the traversing mechanism) and at various positions until completely withdrawn.

2.4. *Pitot-Tube Size.*—In traverses of subsonic boundary-layers the errors introduced by the use of a pitot-tube have been analysed by several workers[2,3,4]. Two main errors, not necessarily independent, were distinguished; the first due to viscosity effects in the flow round the pitot-tube and present only at low values of the Reynolds number based on the tube radius, the second due to the presence of total pressure gradients normal to the flow direction.

With no pressure gradients present it has been demonstrated[2] that errors due to viscosity effects are negligible for values of $ru/\nu > 30$, where ν is the kinematic viscosity and u the velocity in the undisturbed field at the point under consideration and r is the radius of the pitot-tube. Although this result clearly depends to some extent on the pitot-head shape and does not apply directly at supersonic speeds it suggests that no viscosity effects of this kind should be present in the tests of this report, since ru/ν is always of the order of 300 or above.

In subsonic tests, at a high enough Reynolds number, the effect of total-head gradient at right-angles to the flow direction can be represented by a shift in the effective centre of the pitot[4]. A similar effect is to be expected in a supersonic flow. Other errors are to be expected when the pitot-tube is very close to the wall.

In order to determine the effects of finite size of the pitot-tubes, traverses of the boundary-layer were made with two different pitot-tubes (*see* Fig. 6 (c) and (d) and the comparison in Fig. 10 (a). A large effect of tube size was found when the distance from the centre of the pitot and the wall was less than one tube diameter (or tube width with the flattened tube). For distances equal to or greater than the tube diameter this large effect disappeared and no appreciable effect was measured. The accuracy of the tests is such that an effect such as the displacement of the effective centre by an amount up to about 0·2 diameters might not be shown, but this limited evidence is against an effect of a larger order than this.

These results are confirmed by some traverses made in connection with other tests, not yet published. The relevant data are reproduced in Figs. 10 (b) and (c). One set of traverses for laminar-flow and two sets for turbulent-flow are given. All are for Mach numbers of about 2·4 and the ratio of tube diameter to boundary-layer displacement thickness covered is from 0·3 to 2·5. Inspection of the results confirms that in the turbulent cases there is no major distortion of the profile in the neighbourhood of the wall when the centre of the pitot is more than one tube diameter from the surface. For the laminar-profiles the evidence is less clear but again the results seem consistent at distances greater than one diameter. At distances of less than one diameter the shift of the curves in the turbulent case seems opposite to that in the laminar case.

Inspection also shows a sufficiently good agreement between the profiles to conclude that the effective centre is not very far removed from the geometric centre, but the slight inconsistencies in the shapes of the individual profiles prevent an accurate analysis of the shift. The scatter is minimised by a shift of the effective centre from the geometrical centre of the order of 0·2 diameters in the direction of increasing velocity.

In a more detailed investigation the possible effects of geometrical shape of the pitot-tube and of Mach number on the shift of effective centre would have to be investigated.

2.5. *Assumption of Two-dimensional Boundary-layer Flow.*—Because of the large length of the wind-tunnel relative to its cross-section, it was considered necessary to check whether the

flow in the boundary-layer could be assumed to be two-dimensional. A cranked pitot-tube, Fig. 6 (b), was used to obtain a traverse 0·43 in. from the wall centre-line and the result is compared with the centre-line traverse in Fig. 11, for traverse position C. The agreement in the shape of the boundary-layer profiles is satisfactory except for a zero position error of about 0·01 in. which is presumably due to the visual method of determining the position in which the tube was in contact with the wall. Although several cases of repeated traverses gave no appreciable zero error, an electrical method of determining pitot-tube wall contact would have been more satisfactory.

3. *Measurements of Boundary-layer on the Wind-Tunnel Wall.*—3.1. *Computations.*—The velocity profiles were calculated from the measured pitot pressure distribution and the static pressure, which was assumed constant and equal to the mean value observed throughout the traverse at the nearest station located 0·81 in. upstream. The total temperature was assumed constant in the field. At each of the four positions traverses were repeated two or three times and, as good agreement was obtained, computations were made only for one set of results at each station.

The values of the displacement thickness (δ^*) and the momentum thickness (θ) of the boundary-layer were computed by graphical integration from the expressions

$$\delta^* = \int_0^\delta \left(1 - \frac{\rho u}{\rho_1 u_1}\right) dy \quad .. \quad .. \quad .. \quad .. \quad .. \quad .. \quad .. \quad .. \quad (1)$$

and

$$\theta = \int_0^\delta \frac{\rho u}{\rho_1 u_1}\left(1 - \frac{u}{u_1}\right) dy \quad .. \quad .. \quad .. \quad .. \quad .. \quad .. \quad .. \quad (2)$$

3.2. *Velocity Profiles.*—The velocity profiles as measured at stations A, B, C and D are shown in Figs. 12, 13 in terms of $M^* = u/a^*$, where a^* is the sonic-flow velocity ($a^* = \sqrt{[2\gamma g R T_0/(\gamma + 1)]}$ and constant for T_0 = const.). There is a marked difference between the profile A, which is laminar in character, and turbulent-shaped profiles B, C and D. This is more clearly indicated in dimensionless plots of u/u_1 and y/δ, Fig. 14.

The determination of the boundary-layer thickness δ was in all cases to a certain extent arbitrary. For traverse A, Fig. 14, values of u/u_1 were obtained for δ = 0·040 in. and 0·045 in., and are compared with theoretical laminar boundary-layer profiles[5] on a flat plate with no pressure gradient at $M = \sqrt{10}$ and 2 (for a Prandtl number of 0·733, the value for air). In the same figure velocity distributions at stations B, C and D are compared with the one-seventh power law. It is evident from these comparisons that the velocity profile is nearly laminar at station A and fully-turbulent at B, C and D. The lack of a closer agreement with the theoretical curve in case A can be attributed to the influence of a severe pressure and velocity gradient in the nozzle section and transition from laminar to turbulent flow. In cases B, C and D the measured profiles follow approximately the one-seventh power, incompressible, turbulent boundary-layer distribution.

3.3. *Displacement and Momentum Thickness.*—The results of calculations of displacement and momentum thicknesses of the boundary-layer are given in Table 1 and plotted, for turbulent flow stations B, C and D in Fig. 15, in terms of δ^*/δ and θ/δ versus Reynolds number, based on the free-stream condition and distance from the nozzle throat. For comparison, values obtained from measurements in the National Physical Laboratory 11-in. square tunnel[6] are included and also the results of a traverse in a similar R.A.E. tunnel. Theoretical values of δ^*/δ and θ/δ at a Mach number of 2·5 and for 1/5, 1/7 and 1/9 power law distributions are also indicated.

TABLE 1

Displacement and Momentum Thickness of Boundary-layer

	Traverse Station	A	B	C	D
x	Distance from nozzle throat (in.)	2·373	8·623	14·873	21·123
$R_N = \frac{\rho_1 u_1 x}{\mu_1}$		6·24 × 10^5	2·19 × 10^6	3·59 × 10^6	5·17 × 10^6
δ	(in.)	0·041	0·18	0·27	0·37
δ^*	(in.)	0·0184	0·0518	0·085	0·11
θ	(in.)	0·00299	0·0118	0·0193	0·0246
δ^*/δ		0·45	0·287	0·315	0·297
θ/δ		0·073	0·0654	0·0715	0·0664

It is apparent from Fig. 15 that over the Reynolds number range investigated the boundary-layer profiles are similar and essentially independent of Reynolds number. The quantitative agreement with the N.P.L. tests is good and by comparison with theoretical values the boundary-layer profiles appear to agree with a power law distribution having an index between 1/5 and 1/7.

4. *Wake Measurements.*—4.1. *Velocity Profiles.*—The same method of calculation of velocity distribution was used for the wake traverses as for the boundary-layer and the velocity profiles are shown in terms of M^* in Fig. 16. In each case test points obtained from two or three traverses are indicated. On original plottings variations in the position of the minimum velocity point and in the actual values of velocity at corresponding points occurred. In order to eliminate these effects, which have little influence on the wake profile, test points were plotted in Fig. 16 in such a manner that the minimum velocity points coincide for various tests. The velocity scale does not represent the actual velocity values, which varied by about 0·03 in M^*, but corresponds to an average common velocity.

From Fig. 16 it is evident that as regards the shape of the wake profiles the method of representation given above is justified, the results of different traverses showing good agreement.

A more serious difficulty, which was not overcome, is the pronounced asymmetry of the wake profiles at stations B, C and D, the degree varying from test to test. This was presumably due to slight inaccuracy in the setting of the central nozzle element and variations in the intensity of disturbances originating from the nozzle exit on the two sides of the wake.

In the case of traverse A, Fig. 16 (a), located only 1·55 in. from the trailing edge, the wake was too narrow to permit an adequate pitot-pressure exploration. In all other cases, B, C and D, the wake profiles were adequately determined and are represented in Fig. 16 (b), (c) and (d). It was found that the profiles on one side only showed a consistent variation with distance x from the nozzle throat and these are drawn for equal free-stream velocity in Fig. 17. Results obtained from two-dimensional multi-nozzle traverses[1] at 11 and 17 in. from the nozzle throat, indicated in Fig. 17, are consistent with the present tests.

Because of the asymmetry of wake profiles the rate of the wake spread could not be determined accurately, but values corresponding to the extreme observed velocity distributions have been collected in Table 2. From the considerations of two dimensional, incompressible fluid wakes it follows that quantities $b/\sqrt{x}$ and bu'_{max} should be constant[7] and independent of x. This is confirmed, at least qualitatively, by Table 2, for traverses at B, C and D.

TABLE 2

Wake Traverses

Traverse	A	B	C	D
Distance from nozzle throat x (in.)	2·373	8·623	14·873	21·123
Half wake-width b (in.)	0·02	0·10 to 0·12	0·12 to 0·15	0·15 to 0·18
Max. velocity deficiency (in terms of M^*) u'_{max}	>0·35	0·046 to 0·06	0·028 to 0·044	0·04 to 0·05
$bu'_{max}.10^4$ in.	—	46 to 72	33 to 66	60 to 90
$b/\sqrt{x}$ in.$^{1/2}$	0·0123	0·033 to 0·041	0·031 to 0·039	0·0326 to 0·0390
D_{f1} lb/in.	0·049 to 0·041	0·0434 to 0·0402	0·051 to 0·031	0·058 to 0·046

4.2. *Experimental and Theoretical Determination of Drag of Central Nozzle Element.*—From the wake traverses the drag of the central nozzle element was determined and compared with theoretical calculations for a flat plate and for the actual nozzle element (taking into account pressure and velocity gradients).

The drag was taken as equal to

$$D_f = \rho_1 u_1^2 S - \int_S \rho u^2 \, dS \qquad (3)$$

where $S = 2bl$ with b = half wake-width, l = element span, u and ρ velocity and density in the wake and u_1, ρ_1 — in the free stream.

This drag arises from the surface friction of the boundary-layer along the nozzle element and appears as a deficiency of momentum in the traverse across the wake. As the deficiency of momentum is calculated relative to the supersonic free-stream momentum the measured drag does not include the pressure drag of the nozzle element. The error in assuming the drag to be entirely due to skin friction is caused by the presence of the boundary-layer along the nozzle element which affects the parameters of the supersonic free stream. With the extremely small boundary-layer thickness encountered on the nozzle profile, this effect is very small at $M = 2·5$; thus the measured drag is subsequently termed frictional drag.

The main difficulty and source of error in the experimental determination of D_f was again due to the asymmetry of the wake profiles and difference in the values of the dynamic pressure at the two-wake boundaries. In the calculations, a mean value of $\rho_1 u_1^2$ was assumed; the results are given in Table 2 in terms of frictional drag force per in. of span, D_{f1}, and extreme values obtained from three or four different traverses at each station are indicated. In the case of traverse A a complete wake profile could not be obtained, *cf.* Fig. 16, and a minimum wake velocity had to be assumed. In view of fluctuations of static pressure along the tunnel, its effect on the calculated magnitude of D_{f1} was investigated and was found to be small: a change of 17 per cent in the static pressure resulted in 2·8 per cent change in D_{f1}. This is due to the fact that for a given pitot pressure the dynamic pressure $\frac{1}{2}\rho u^2 = \gamma P M^2/2$ is insensitive to P, the Mach number varying in opposite direction to the static pressure.

The calculated values of D_{f1}, Table 2, vary between 0·058 and 0·031 lb/in. It appears that the most reliable results were obtained at station B, at which particularly good repeats of the wake profile were recorded, Fig. 16 (b): the four values of D_{f1} were equal to 0·0434, 0·0422, 0·0417, 0·0402, from which $D_{f1\,mean} = 0·0418$.

The above experimental results were compared with theoretical estimates. In the first instance values of D_{f1} were obtained on the assumption of flat plate, zero pressure gradient, laminar-flow and free-stream conditions corresponding to sonic velocity and Mach number of 2·5, at the nozzle exit. The friction coefficient c_f was assumed to be given at these Mach numbers by $c_f \sqrt{R_N} = 1{\cdot}30$ and $1{\cdot}24$, respectively[8] and D_{f1} was found to be 0·027 lb/in. and 0·022 lb/in., *i.e.*, about half of the experimental value. Considering the existence of very high pressure and velocity gradients over the nozzle element surface, the above result was not unexpected and a more refined method of calculation was subsequently employed.

The skin frictional drag of the nozzle profiles was calculated according to the method given in Ref. 9 which extends the Pohlhausen solution for a laminar boundary-layer to cover compressible flow.

A brief outline of the assumptions and method is given below. For steady flow the Kármán momentum equation is obtained and may be written

$$\frac{d}{dx}\left(\rho_1 u_1^2 \theta\right) + \rho_1 u_1 \frac{du_1}{dx}\,\delta^* = \mu_w \left(\frac{\partial u}{\partial y}\right)_w \quad .. \quad .. \quad .. \quad .. \quad .. \quad .. \quad (4)$$

where δ^* and θ are respectively the displacement thickness and momentum thickness defined by equations (1) and (2), with $(\ )_1$ referring to the free stream and $(\ )_w$ — to conditions at the wall.

The assumptions now made are

(a) The velocity distribution may be given as a polynomial satisfying certain end conditions (Hartree profiles are chosen in Ref. 9).

(b) $P_r = 1$ and no heat transfer occurs, thus the wall temperature is equal to the stagnation temperature and the density distribution may be written in terms of the velocity distribution.

Equation (4) may be written

$$u_1 \frac{d}{dx}\left(\frac{\rho_1 \theta^2}{\mu_w}\right) + \frac{\rho_1 \theta^2}{\mu_w} \cdot \frac{du_1}{dx}\left(2\,\frac{\delta^*}{\theta} + 4 - M_1^2\right) = 2\left(\frac{\partial}{\partial(y/\theta)} \cdot \frac{u}{u_1}\right)_w \quad .. \quad .. \quad (5)$$

The parameter $\lambda^* = -\left(\dfrac{\partial^2}{\partial(y/\delta)^2} \cdot \dfrac{u}{u_1}\right) = \dfrac{\rho_1 \theta^2}{\mu_w} \cdot \dfrac{du_1}{dx}$ is now defined and the components of equation (5) may be expressed in terms of λ^*.

From the quantities $\dfrac{\delta^*}{\theta}$ and $\left(\dfrac{\partial}{\partial(y/\theta)} \cdot \dfrac{u}{u_1}\right)_w$ as functions of λ^*, the skin frictional drag is found by numerical integration.

This method was applied to the surface of the nozzle profile (Fig. 4). The velocity gradient along the surface is given in Fig. 18. The flow from the forward stagnation point over the initial cylindrical surface was taken from flow over a cylinder and thereafter a one-dimensional flow was assumed as far as the throat. The surface velocities in the supersonic region were obtained by the method of characteristics.

The incompressible solution for skin frictional drag over a cylinder provides a starting point for a step-by-step integration of equation (5). Eight stages were taken in the calculation and the variation of skin frictional force is given in Fig. 18. By this means a frictional drag of the profile of 0·0464 lb/in. is obtained which compares very well with the experimental value of 0·042 lb/in.

It is seen from Fig. 18 that a very sharp change of velocity gradient occurs at the point of inflexion of the profile. In this nozzle, the radius at the throat is equal to the throat gap and the circular-arc is maintained as far as the point of inflexion. The calculation shows that the sudden decrease in velocity gradient at the point of inflexion causes rapid thickening of the boundary-layer. As stated in section 2.3, recent pressure traverses on similar nozzles have indicated that this gives rise to an expansion disturbance of appreciable intensity followed by re-compression, which has a marked detrimental effect on the pressure distribution along the nozzle axis.

This difficulty has been eliminated on recently-designed nozzles by using a long throat section so shaped as to avoid sudden changes in velocity gradient.

5. *Conclusions.*—(1) Both the laminar and turbulent boundary-layer profiles were traversed and found to be well defined and distinct. The laminar profile is in reasonable agreement with the theoretical profile and it is probable that transition occurs close to the plane of traverse. The turbulent profiles are in close agreement with those obtained in other tunnels and conform to the one-seventh power law distribution.

(2) The experimental characteristics of the wake (rates of spread and decay) are in agreement with those of an incompressible wake.

(3) The measured wake drag compares very well with that calculated from considerations of laminar boundary-layer growth along the nozzle surface.

(4) Experimental and theoretical results indicate that the shape of the nozzle profile, particularly at the point of inflexion, must be such as to avoid sudden changes of velocity and pressure gradient. This is particularly important on nozzles designed with short throat sections.

LIST OF SYMBOLS

a^*	Sonic-flow velocity $(= \sqrt{[2\gamma g R T_0/(\gamma + 1)]})$
b	Half-wake width
D_f	Frictional drag
D_f/l	Span of nozzle element
M	Mach number
$M^* = u/a^*$	
P	Static pressure
P_0	Stagnation pressure
P_0'	Pitot pressure
R_N	Reynolds number (based on distance from nozzle throat and free-stream conditions)
S	$2bl$

LIST OF SYMBOLS—*continued.*

T_0	Stagnation temperature
u	Velocity
u'_{max}	Maximum velocity deficiency in the wake
x	Distance from the nozzle throat
y	Distance measured from the wall and normal to the wall
γ	$= C_P/C_v = 1{\cdot}400$
δ	Boundary-layer thickness
δ^*	Boundary-layer displacement thickness
θ	Boundary-layer momentum thickness
μ	Viscosity
$( )_1$	Conditions in the free stream outside the boundary-layer
$( )_w$	Conditions at the wall.

REFERENCES

No.	*Author*	*Title, etc.*
1	J. K. Royle, A. G. Bowling, and J. Lukasiewicz	Calibration of Two-dimensional and Conical Supersonic Multi-nozzles. A.R.C. 11,039. 1947. (Unpublished).
2	Miss M. Barker	On the Use of Very Small Pitot-tubes for Measuring Wind Velocity. *Proc. Roy. Soc.* A.101, p. 435. 1922.
3	G. I. Taylor	Measurements with a Half Pitot-Tube. *Proc. Roy. Soc.* A.166, p. 476. 1938.
4	A. D. Young and J. N. Maas ..	The Behaviour of a Pitot Tube in a Transverse Total Pressure Gradient. R. & M. No. 1770. Sept., 1937.
5	Emmons and Brainerd	Effect of Variable Viscosity on Boundary Layers, with a Discussion of Drag Measurements. *J. Applied Mechanics*, 1942.
6	W. F. Cope and G. G. Watson ..	Preliminary Measurements of the Boundary Layer in the 11 in. Supersonic Wind Tunnel. N.P.L. ENG. DIV. 233/46. August, 1946.
7	L. Prandtl	The Mechanics of Viscous Fluids. Aerodynamic Theory, ed. Durant, Vol. 3, Div. 6.
8	Kármán and Tsien	Boundary Layer in Compressible Fluids. *J. Ae. Sci.*, 1938.
9	K. Oswatitsch and K. Wieghardt ..	Theoretical Investigations on Steady Potential Flows and Boundary Layers at High Speeds. A.R.C. 10378. 1946. (Unpublished).

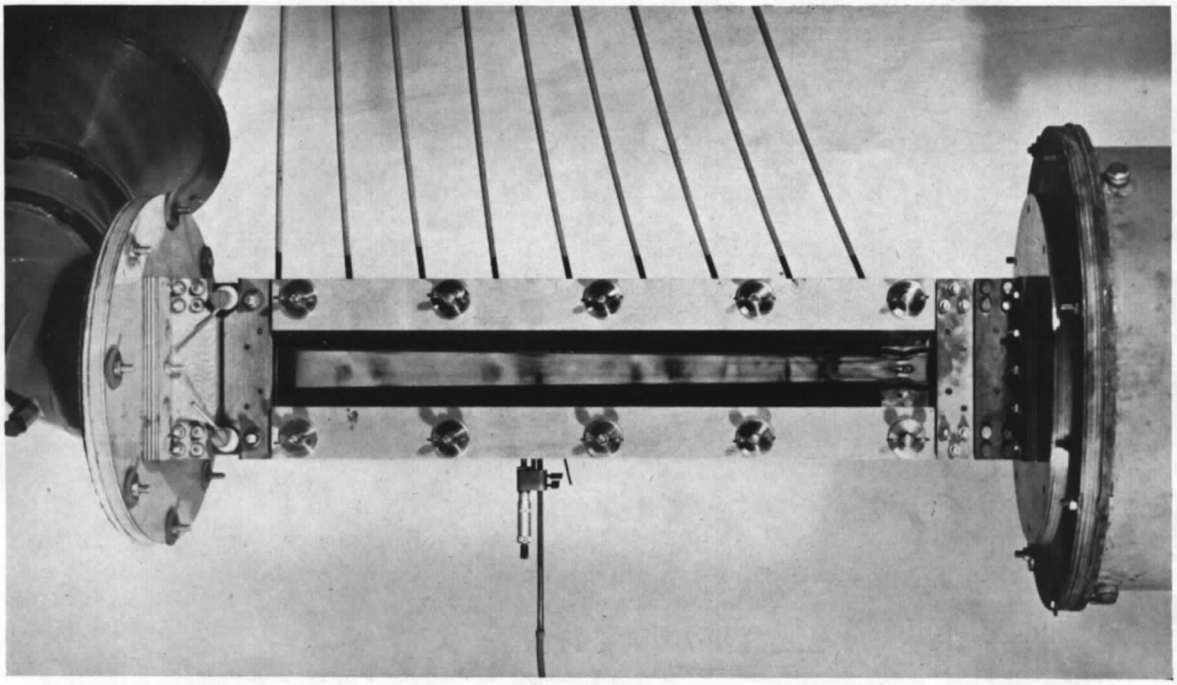

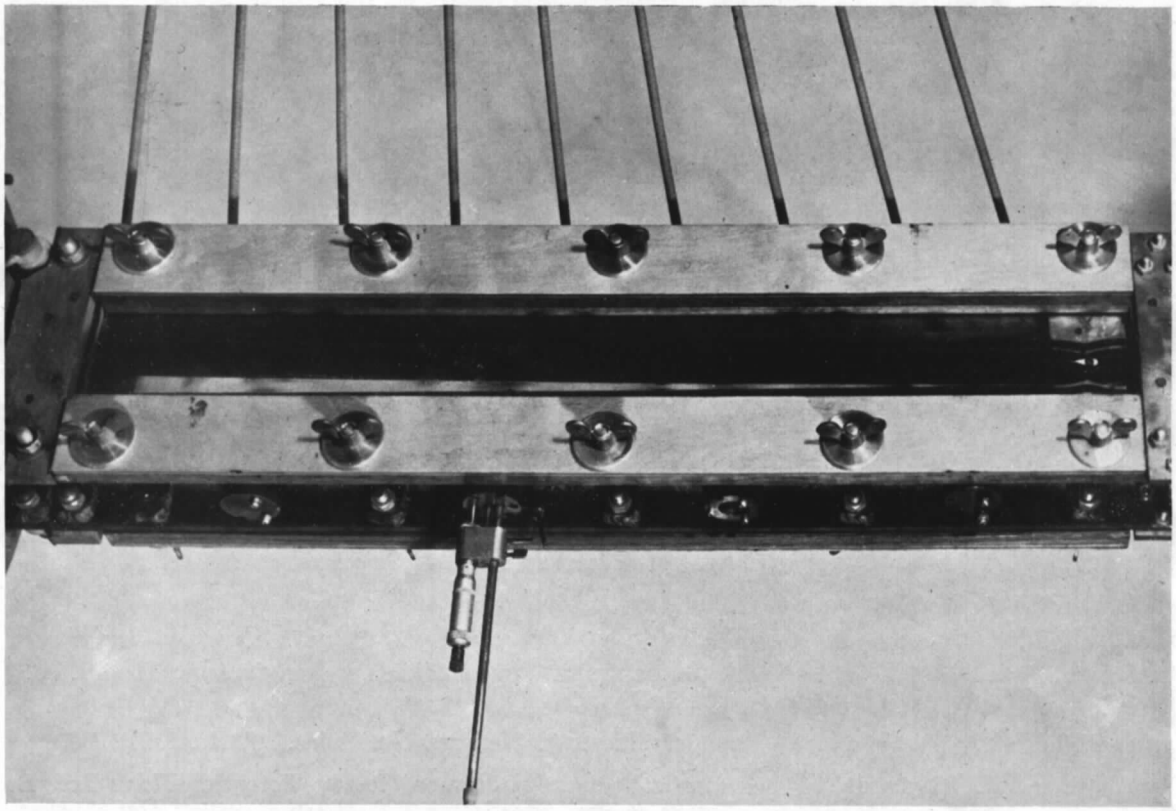

FIGS. 1 and 2. Supersonic tunnel.

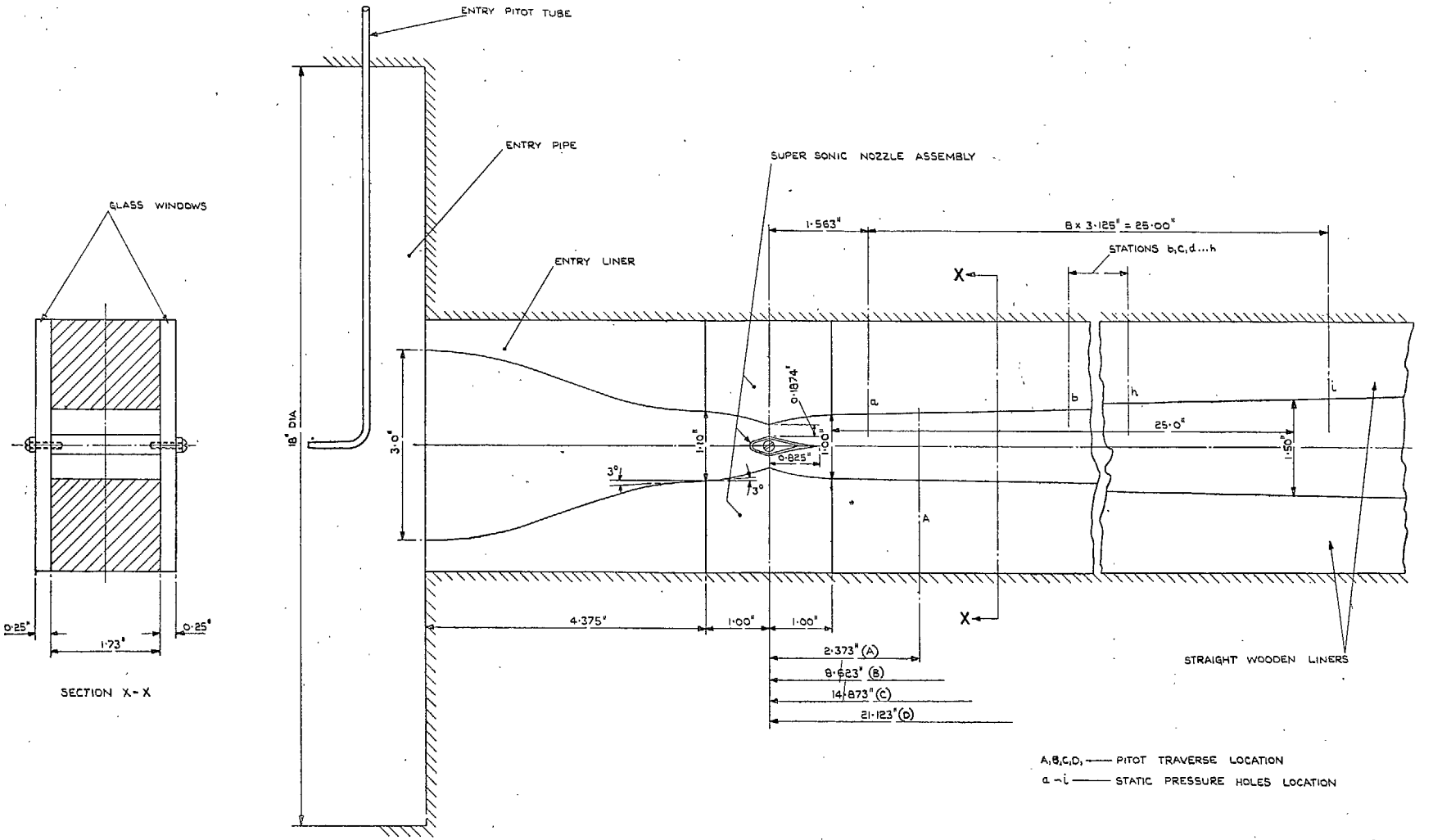

FIG. 3. General arrangement of supersonic tunnel.

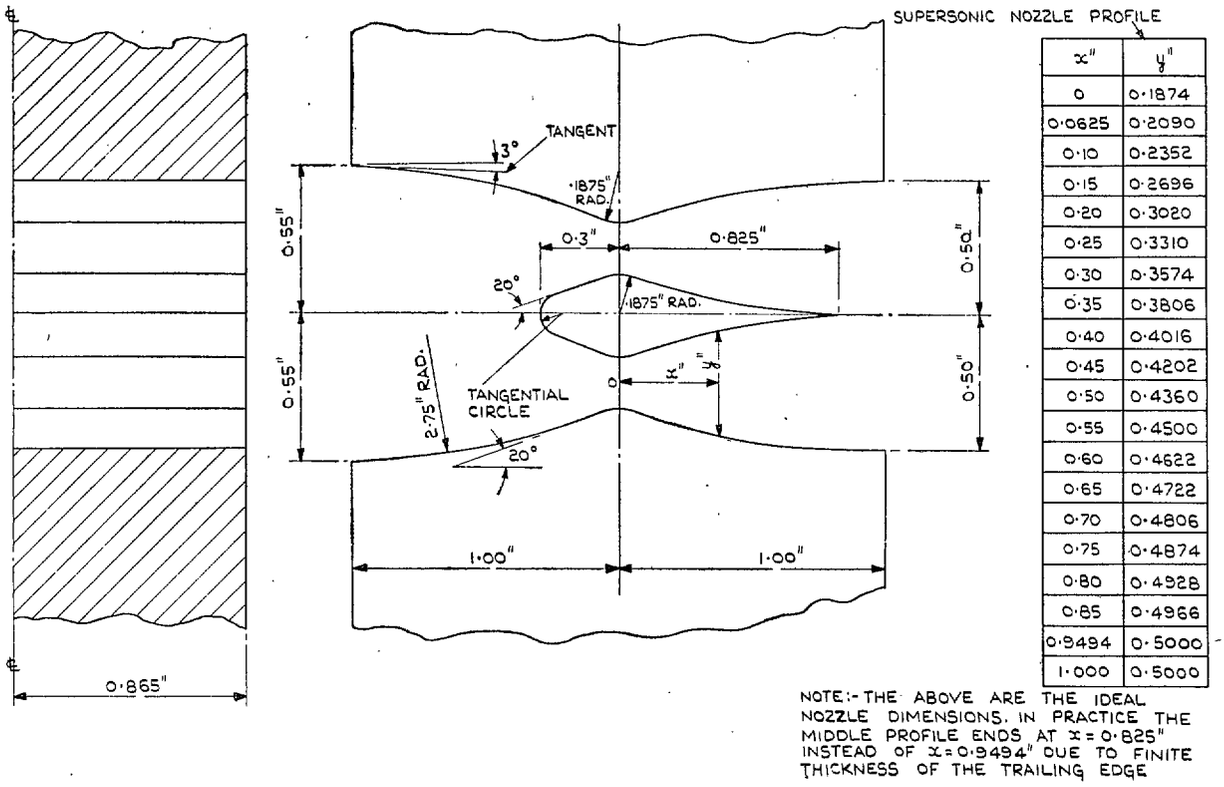

x"	y"
0	0·1874
0·0625	0·2090
0·10	0·2352
0·15	0·2696
0·20	0·3020
0·25	0·3310
0·30	0·3574
0·35	0·3806
0·40	0·4016
0·45	0·4202
0·50	0·4360
0·55	0·4500
0·60	0·4622
0·65	0·4722
0·70	0·4806
0·75	0·4874
0·80	0·4928
0·85	0·4966
0·9494	0·5000
1·000	0·5000

FIG. 4. Supersonic nozzle assembly.

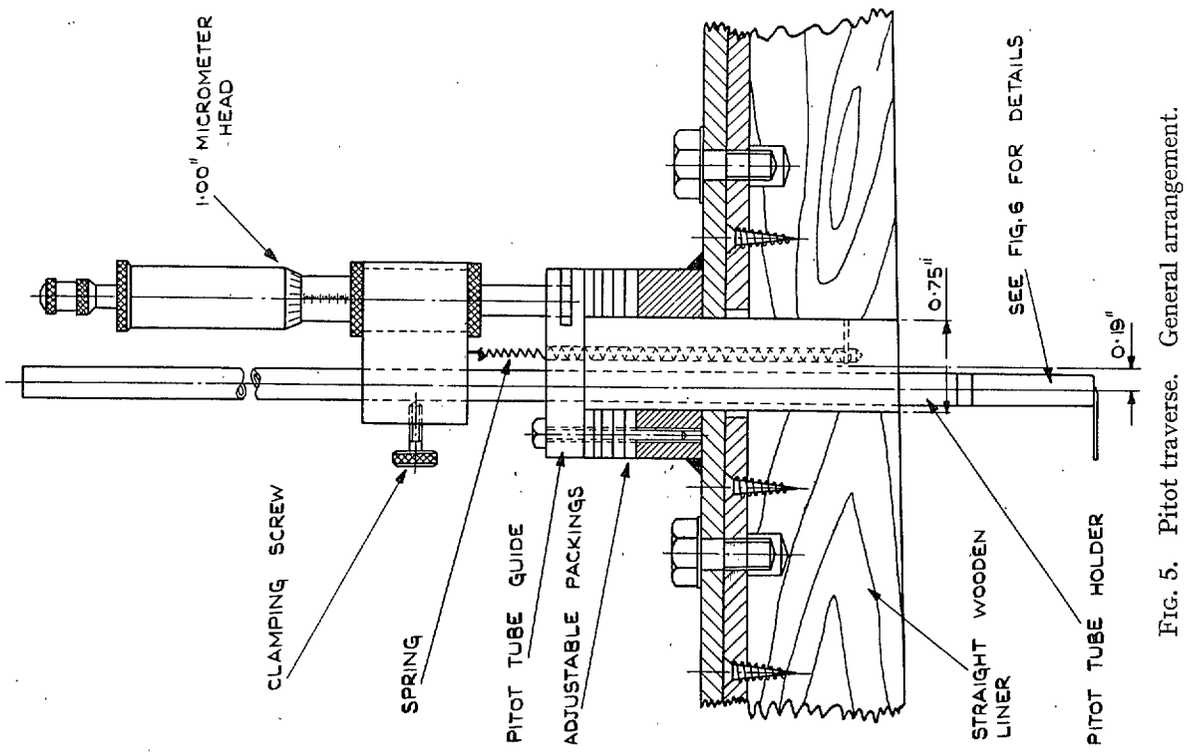

FIG. 5. Pitot traverse. General arrangement.

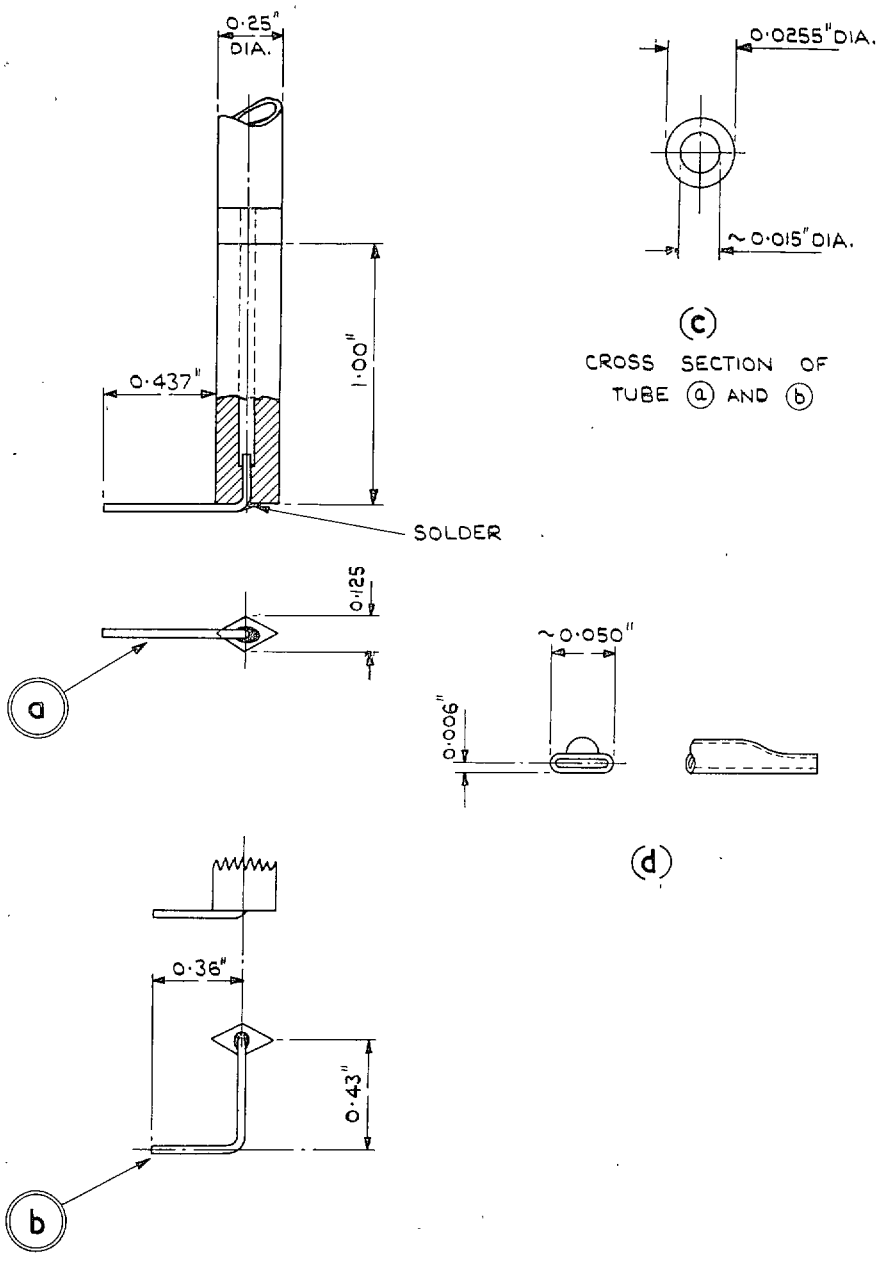

FIG. 6 (a-d). Pitot traverse. Tube details.

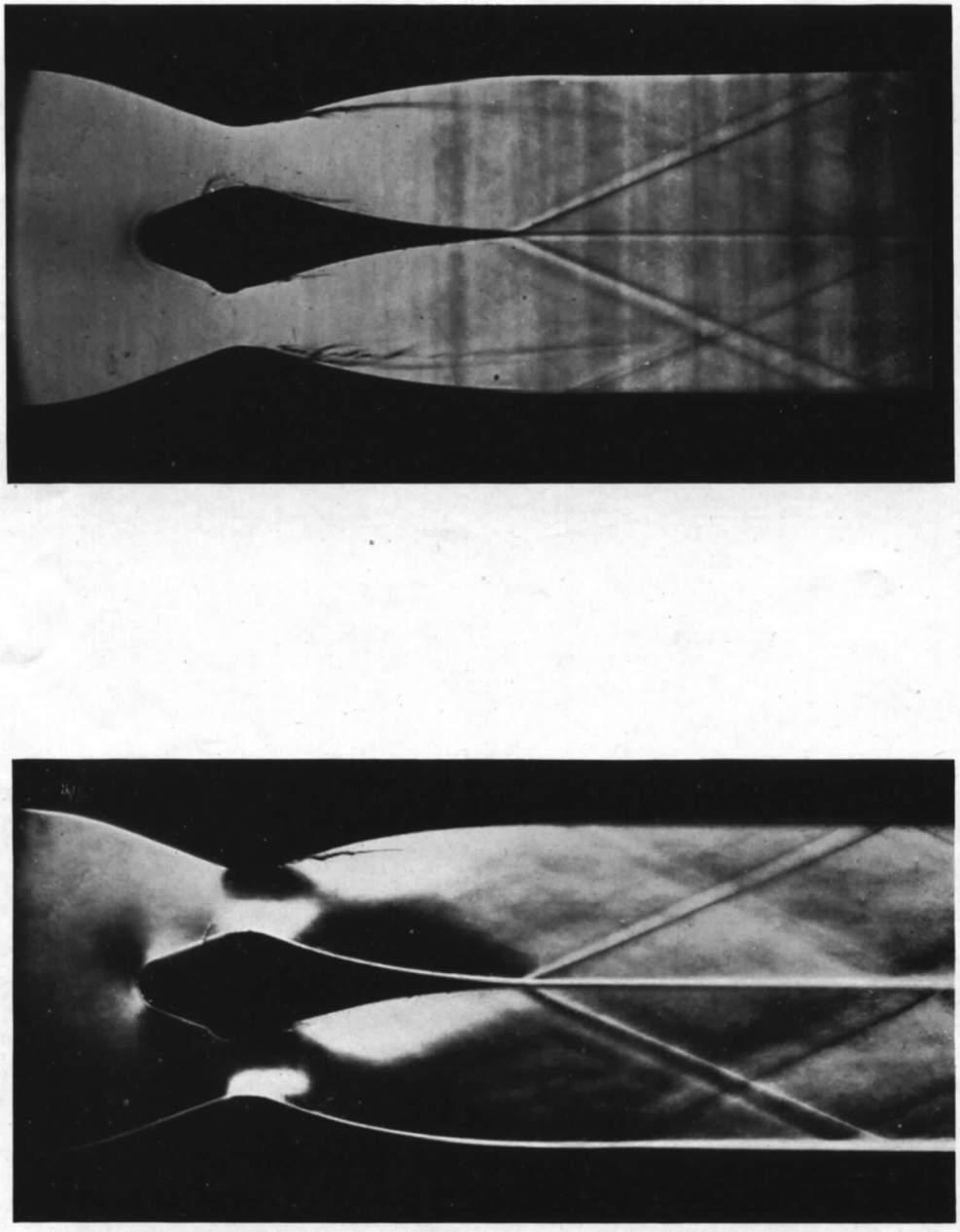

FIG. 7. Shadow and schlieren photographs of flow in the nozzle.

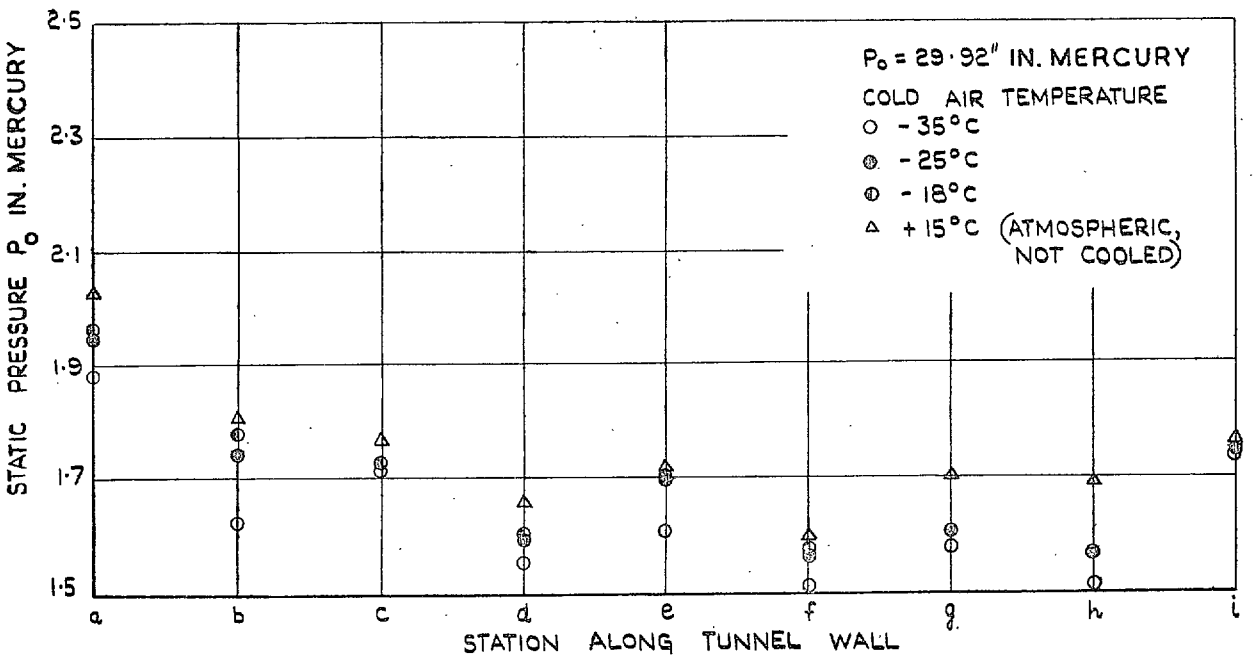

FIG. 8. Static pressure distribution (empty tunnel, dry and humid air).

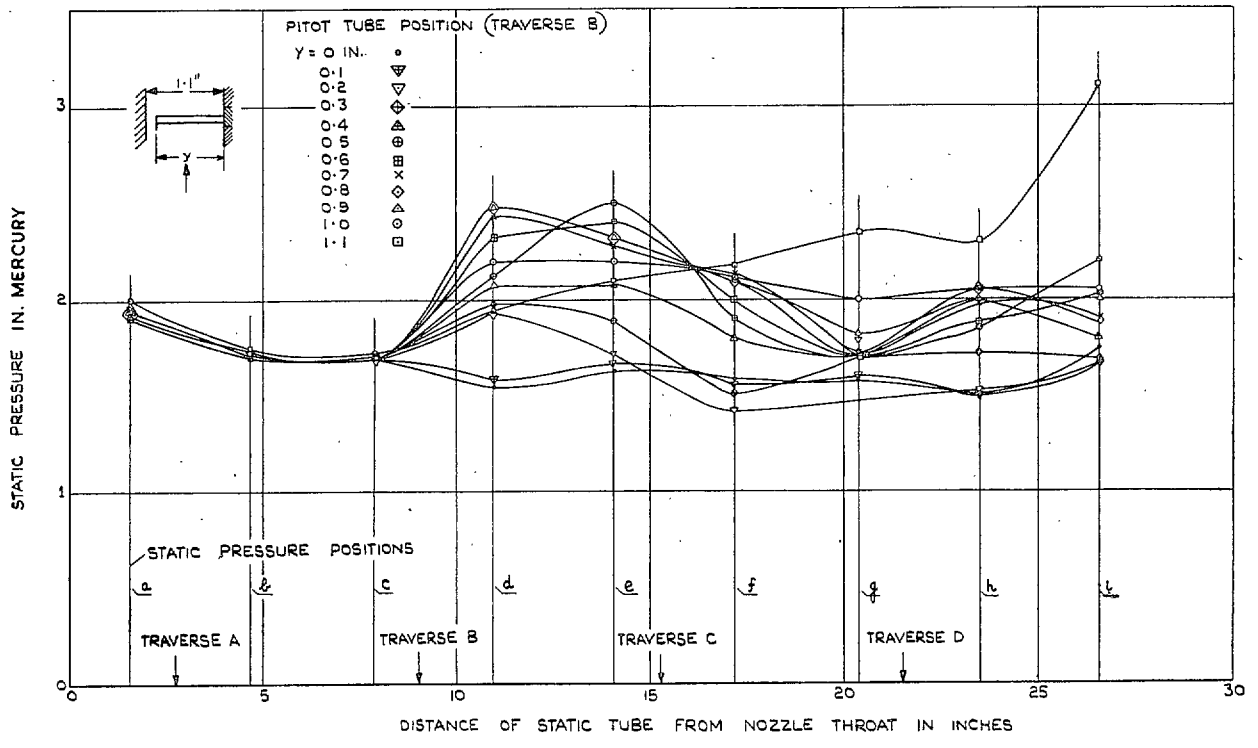

FIG. 9. Effect of pitot-tube position on static pressure distribution.

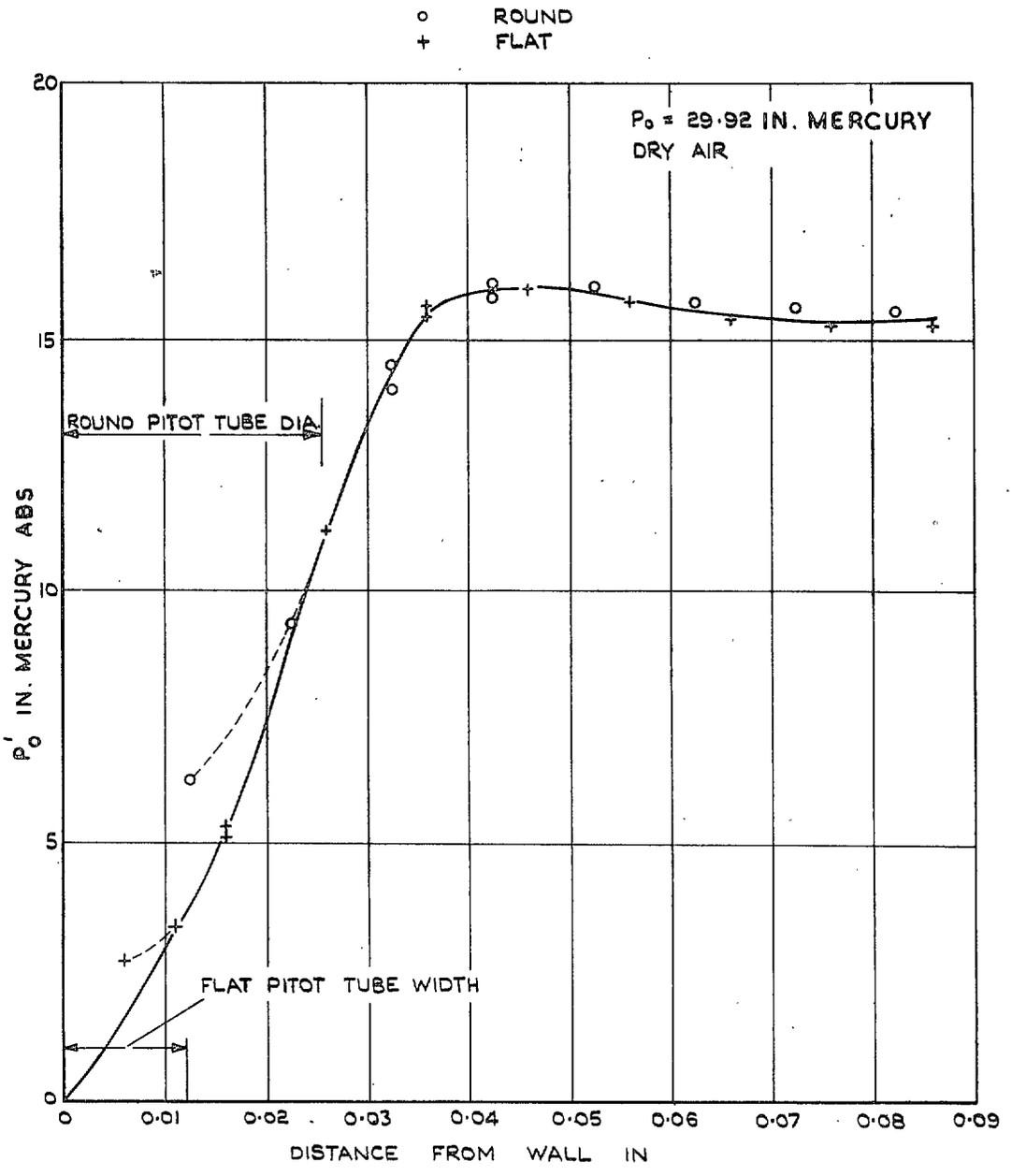

FIG. 10 (a). Effect of pitot-tube size on boundary-layer measurement (traverse A).

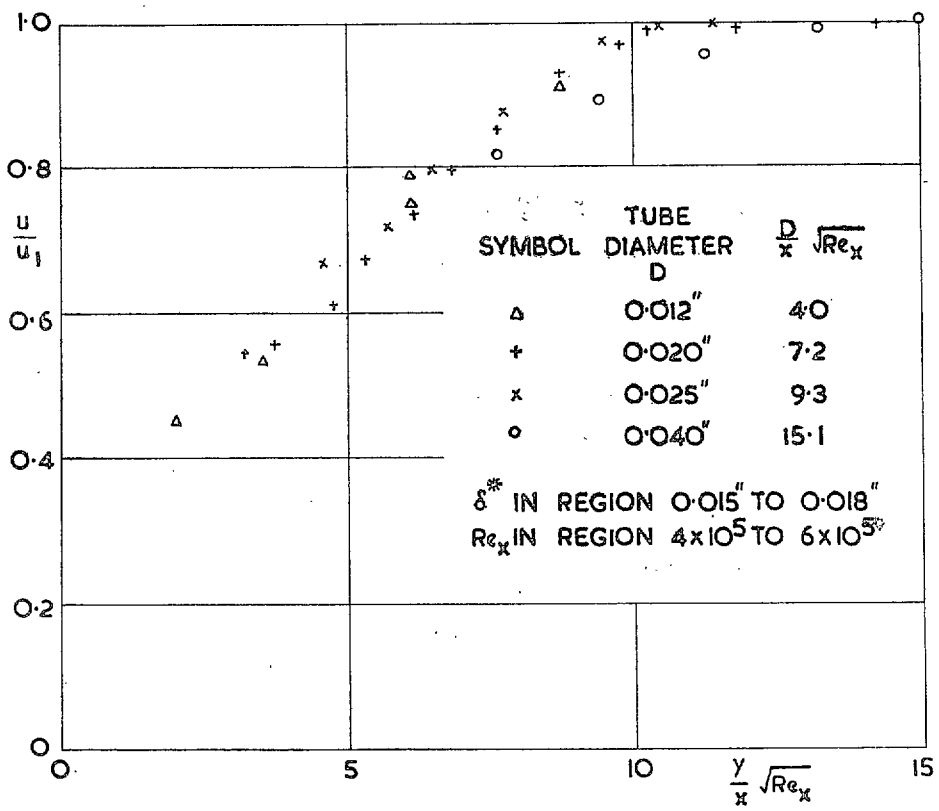

FIG. 10 (b). Velocity distributions in a laminar boundary-layer as measured by different sizes of pitot-tube.

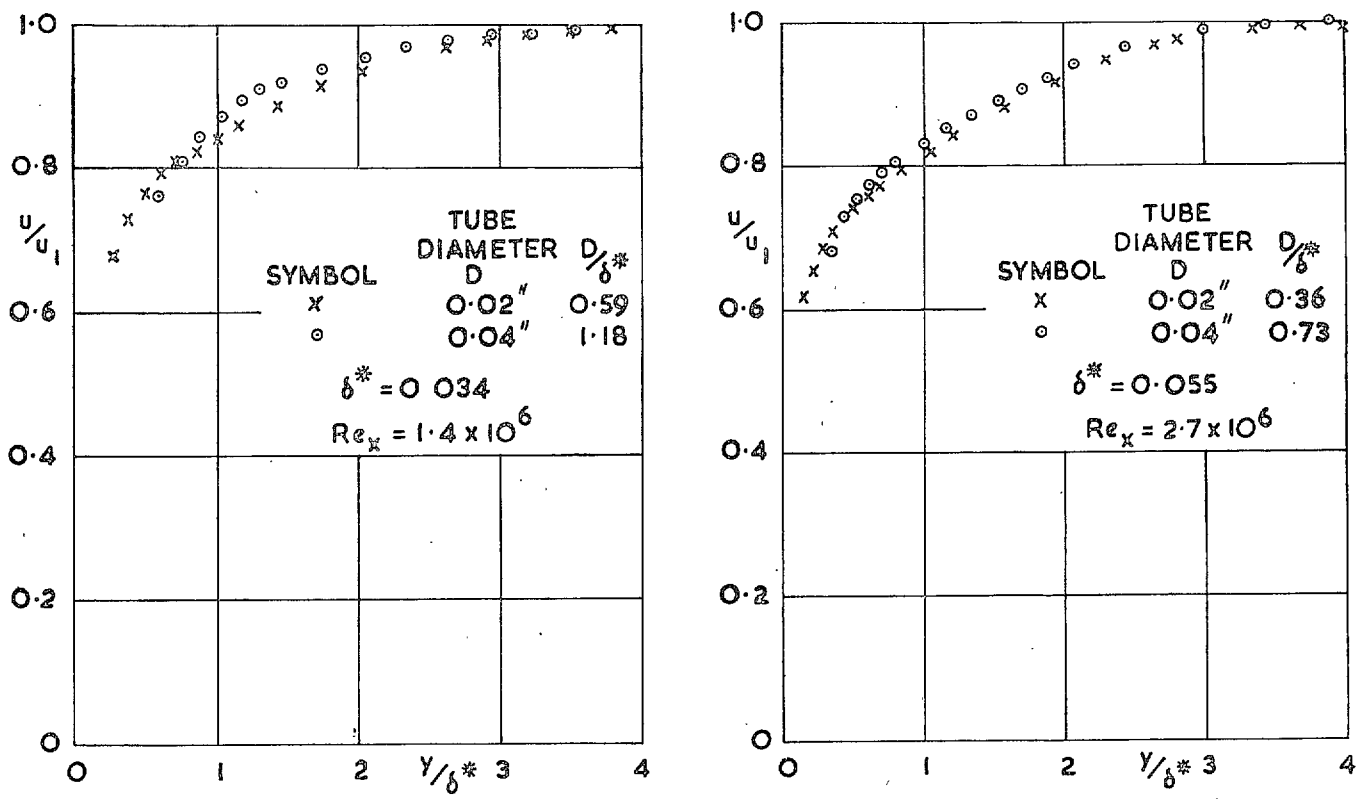

FIG. 10 (c). Velocity distributions in a turbulent boundary-layer as measured by two sizes of pitot-tube. (δ* displacement thickness).

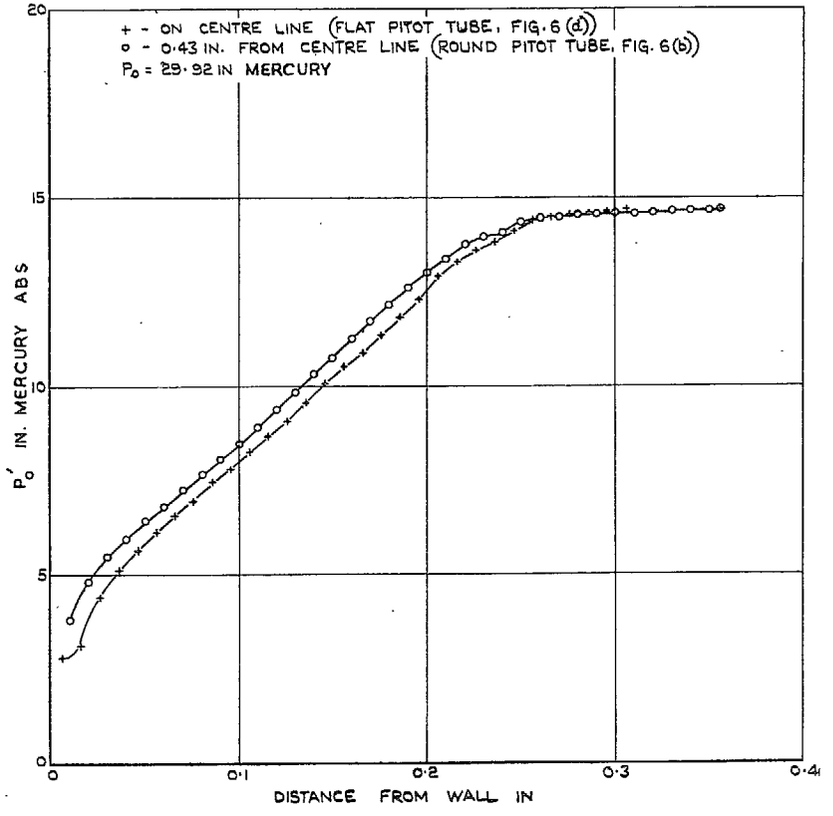

FIG. 11. Boundary-layer traverse in the wall centre-line plane and 0·43 in. off the centre-line (traverse C).

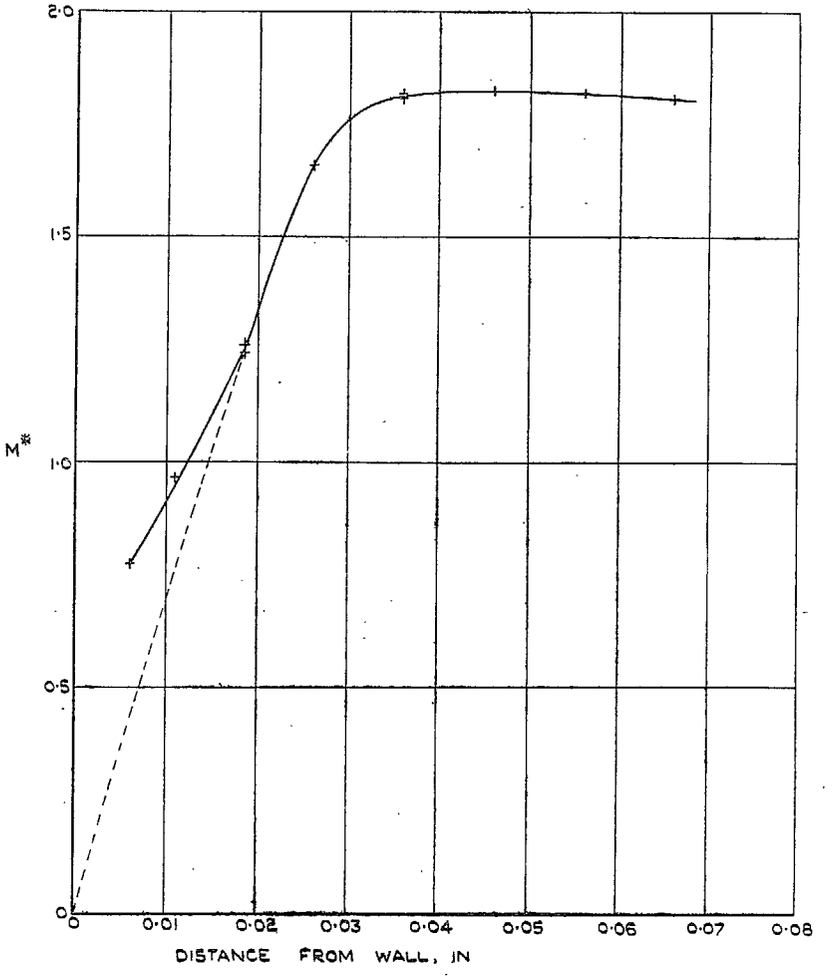

FIG. 12. Velocity distribution in boundary-layer, station A.

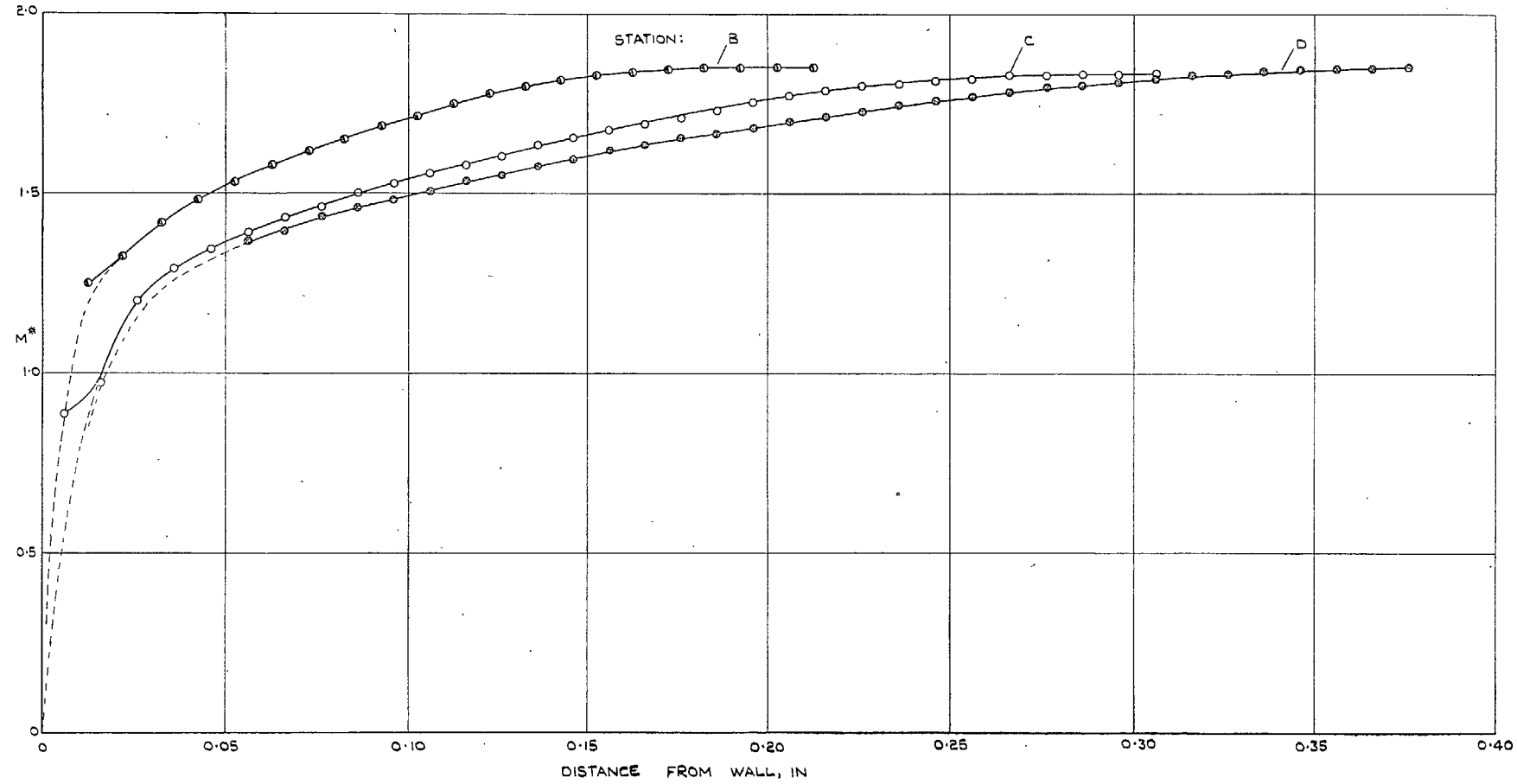

FIG. 13. Velocity distribution in boundary-layer at stations B, C, D.

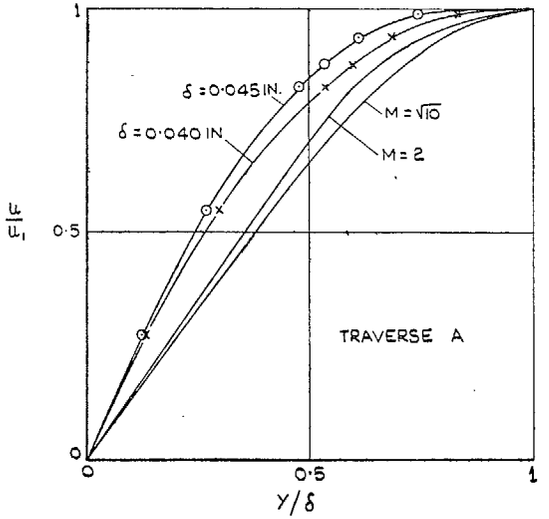

THEORETICAL COMPRESSIBLE LAMINAR BOUNDARY LAYER PROFILES COMPARED WITH EXPERIMENTAL PROFILE AT STATION A

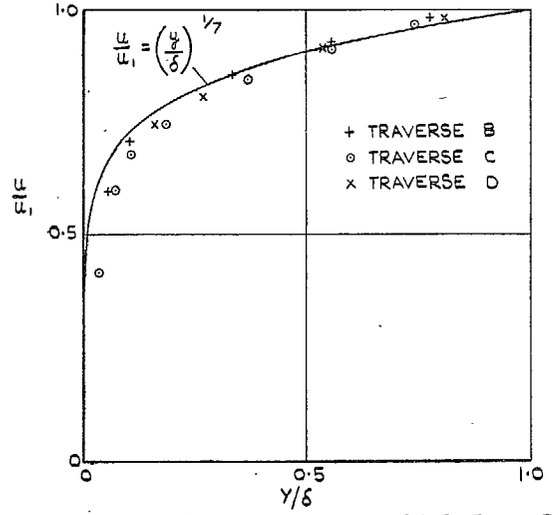

COMPARISON OF THEORETICAL INCOMPRESSIBLE TURBULENT BOUNDARY LAYER PROFILE (1/7 POWER LAW) WITH EXPERIMENTAL PROFILES AT STATIONS B,C AND D.

FIG. 14. Dimensionless boundary-layer profiles.

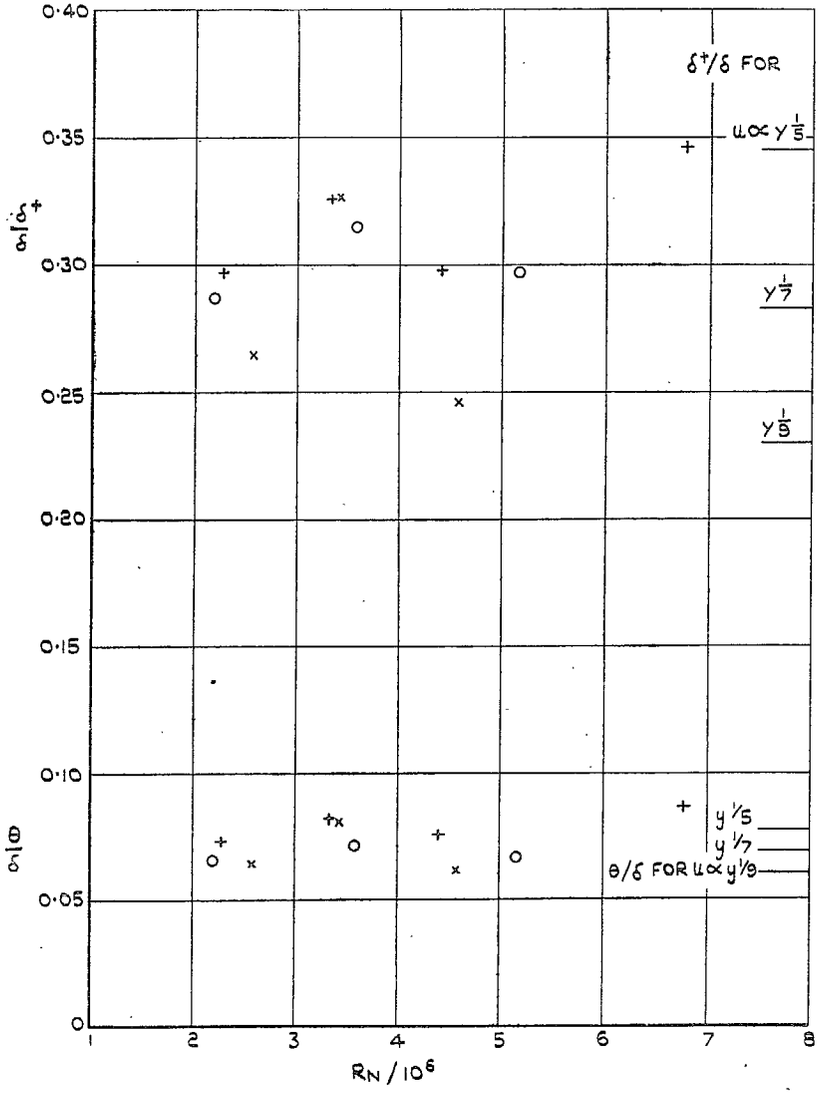

FIG. 15. δ^*/δ and θ/δ as functions of R_N (based on free-stream conditions and distance from nozzle throat).
O R.A.E. and + N.P.L. tests, × further R.A.E. tests in similar tunnel at $M = 2{\cdot}5$.

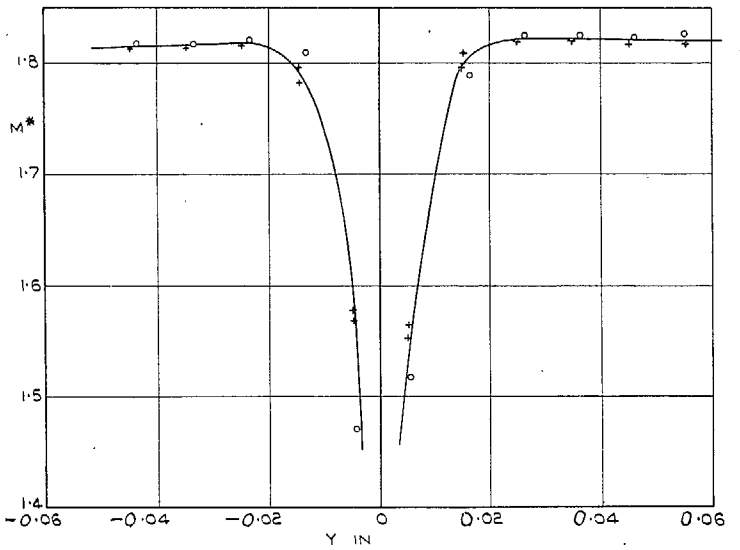

(a) WAKE TRAVERSE AT STATION A

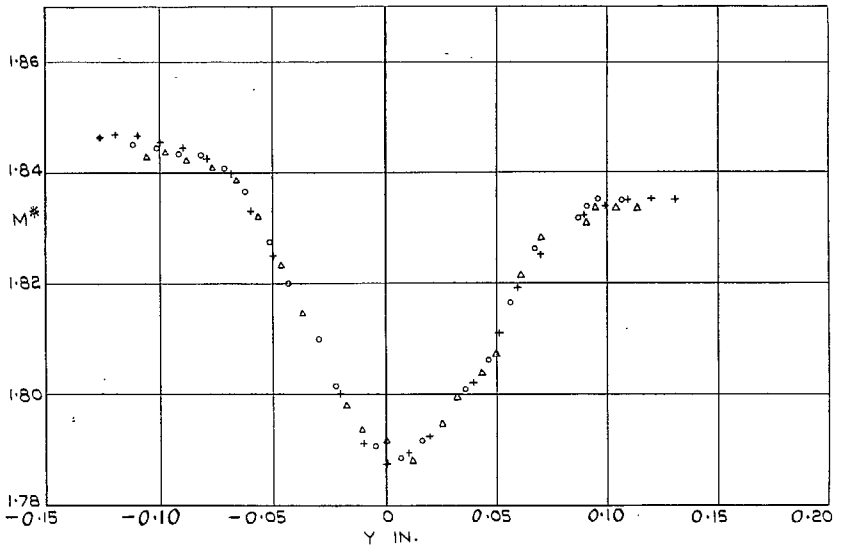

(b) WAKE TRAVERSE AT STATION B

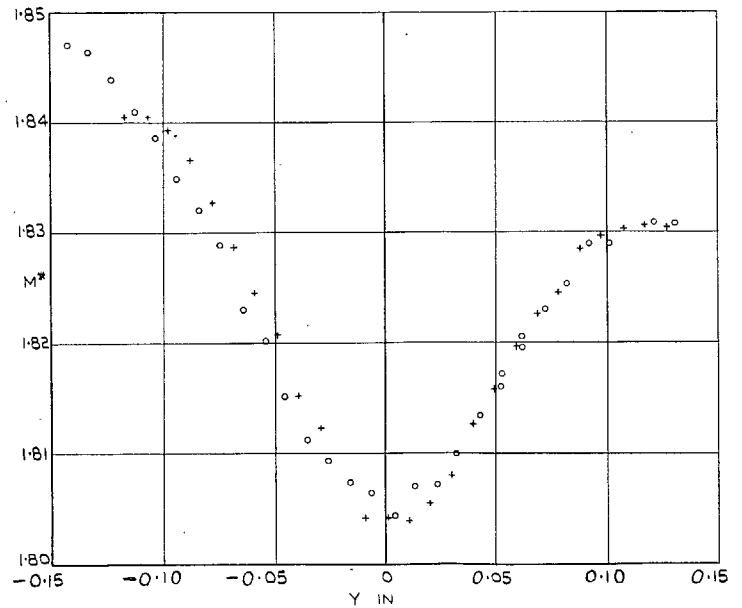

(c) WAKE TRAVERSE AT STATION C

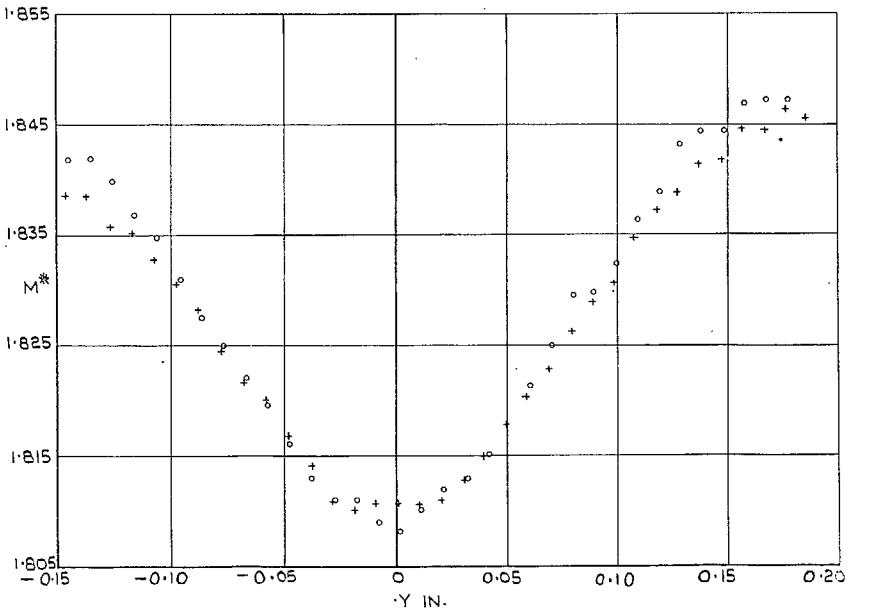

(d) WAKE TRAVERSE AT STATION D

FIG. 16 (a-d). Wake traverses.

(22306) Wt. 15-680 K9 1/52 F. M. & S.

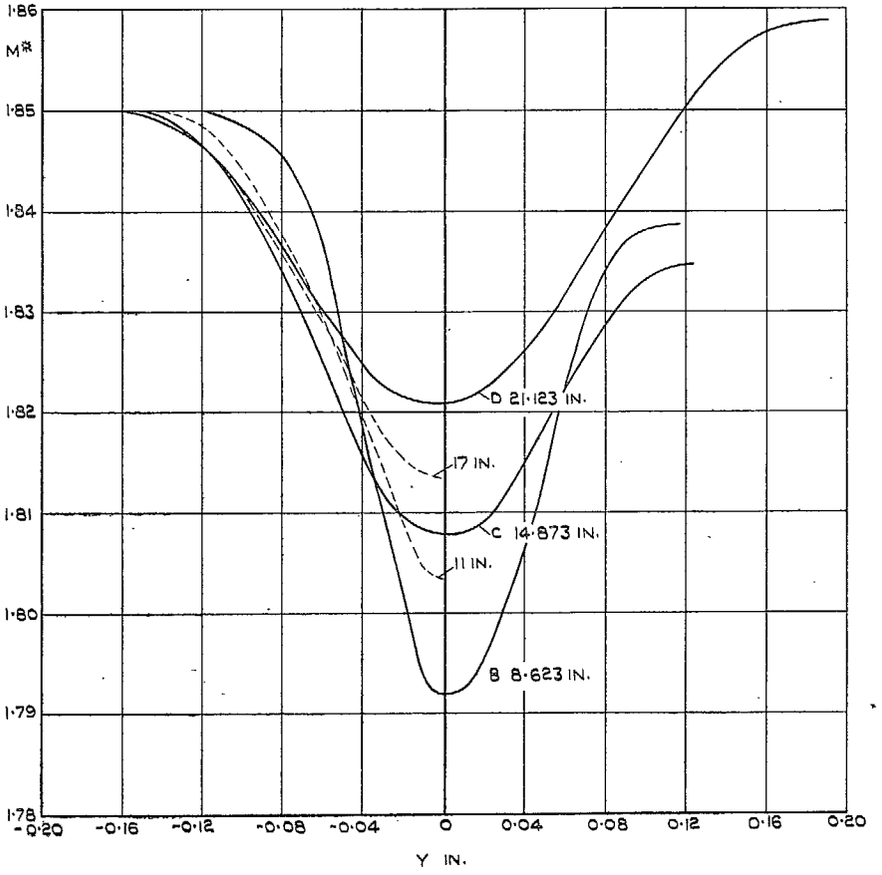

FIG. 17. Wake profiles at B, C, D.
(Distances from nozzle throat indicated;
results from ref. 1 marked thus – – –)

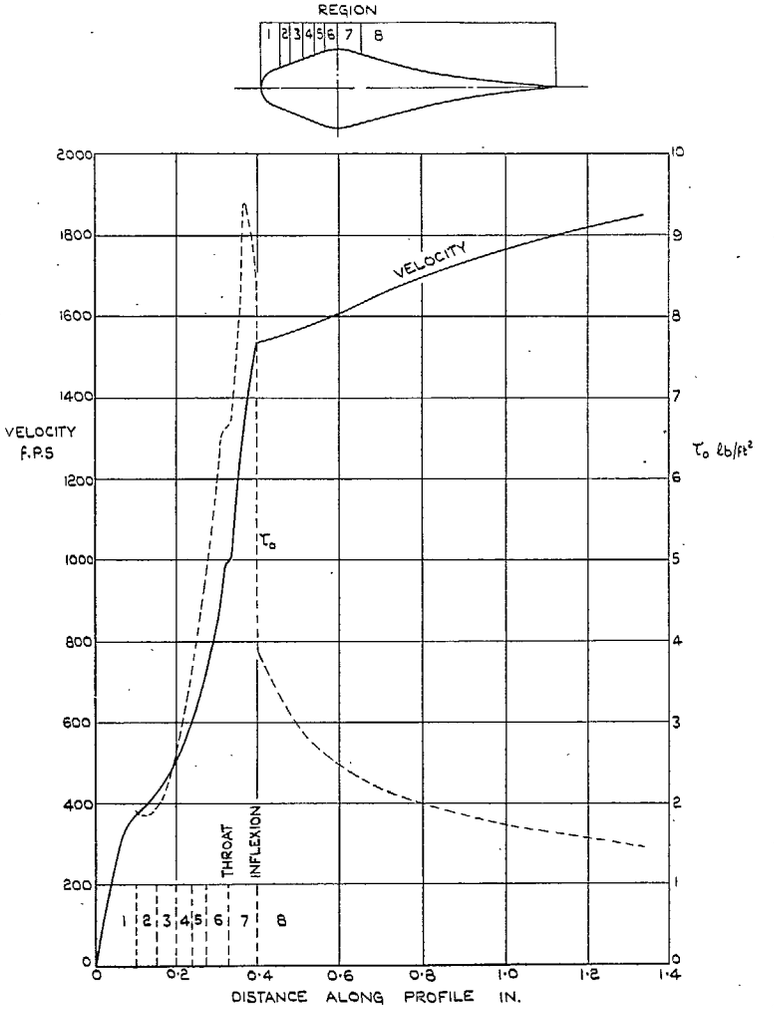

FIG. 18. Velocity and surface friction distribution.

PRINTED IN GREAT BRITAIN

Publications of the Aeronautical Research Council

ANNUAL TECHNICAL REPORTS OF THE AERONAUTICAL RESEARCH COUNCIL (BOUND VOLUMES)—

1934–35 Vol. I. Aerodynamics. *Out of print.*
Vol. II. Seaplanes, Structures, Engines, Materials, etc. 40*s.* (40*s.* 8*d.*)

1935–36 Vol. I. Aerodynamics. 30*s.* (30*s.* 7*d.*)
Vol. II. Structures, Flutter, Engines, Seaplanes, etc. 30*s.* (30*s.* 7*d.*)

1936 Vol. I. Aerodynamics General, Performance, Airscrews, Flutter and Spinning. 40*s.* (40*s.* 9*d.*)
Vol. II. Stability and Control, Structures, Seaplanes, Engines, etc. 50*s.* (50*s.* 10*d.*)

1937 Vol. I. Aerodynamics General, Performance, Airscrews, Flutter and Spinning. 40*s.* (40*s.* 10*d.*)
Vol. II. Stability and Control, Structures, Seaplanes, Engines, etc. 60*s.* (61*s.*)

1938 Vol. I. Aerodynamics General, Performance, Airscrews. 50*s.* (51*s.*)
Vol. II. Stability and Control, Flutter, Structures, Seaplanes, Wind Tunnels, Materials. 30*s.* (30*s.* 9*d.*)

1939 Vol. I. Aerodynamics General, Performance, Airscrews, Engines. 50*s.* (50*s.* 11*d.*)
Vol. II. Stability and Control, Flutter and Vibration, Instruments, Structures, Seaplanes, etc. 63*s.* (64*s.* 2*d.*)

1940 Aero and Hydrodynamics, Aerofoils, Airscrews, Engines, Flutter, Icing, Stability and Control, Structures, and a miscellaneous section. 50*s.* (51*s.*)

Certain other reports proper to the 1940 *volume will subsequently be included in a separate volume.*

ANNUAL REPORTS OF THE AERONAUTICAL RESEARCH COUNCIL—

1933–34	1*s.* 6*d.* (1*s.* 8*d.*)
1934–35	1*s.* 6*d.* (1*s.* 8*d.*)
April 1, 1935 to December 31, 1936.	4*s.* (4*s.* 4*d.*)
1937	2*s.* (2*s.* 2*d.*)
1938	1*s.* 6*d.* (1*s.* 8*d.*)
1939–48	3*s.* (3*s.* 2*d.*)

INDEX TO ALL REPORTS AND MEMORANDA PUBLISHED IN THE ANNUAL TECHNICAL REPORTS, AND SEPARATELY—

April, 1950 R. & M. No. 2600. 2*s.* 6*d.* (2*s.* 7½*d.*)

INDEXES TO THE TECHNICAL REPORTS OF THE AERONAUTICAL RESEARCH COUNCIL—

December 1, 1936 — June 30, 1939.	R. & M. No. 1850.	1*s.* 3*d.* (1*s.* 4½d.)
July 1, 1939 — June 30, 1945.	R. & M. No. 1950.	1*s.* (1*s.* 1½*d.*)
July 1, 1945 — June 30, 1946.	R. & M. No. 2050.	1*s.* (1*s.* 1½*d.*)
July 1, 1946 — December 31, 1946.	R. & M. No. 2150.	1*s.* 3*d.* (1*s.* 4½*d.*)
January 1, 1947 — June 30, 1947.	R. & M. No. 2250.	1*s.* 3*d.* (1*s.* 4½*d.*)

Prices in brackets include postage.

Obtainable from

HER MAJESTY'S STATIONERY OFFICE

York House, Kingsway, LONDON, W.C.2 423 Oxford Street, LONDON, W.1
P.O. Box 569, LONDON, S.E.1
13a Castle Street, EDINBURGH, 2 1 St. Andrew's Crescent, CARDIFF
39 King Street, MANCHESTER, 2 Tower Lane, BRISTOL, 1
2 Edmund Street, BIRMINGHAM, 3 80 Chichester Street, BELFAST

or through any bookseller.